– For internal NASA and partners use only –

Lunar Impact Ejecta Benchmark and Models

Anthony M. DeStefano
NASA, MSFC, EV44

February 19, 2020

Contents

1 Executive Summary **1**

2 Characteristics of the 17 March 2013 Event **1**
2.1 LRO Observations: Robinson et al. 2015 1
2.1.1 Crater Morphology 1
2.1.2 Impact Event Parameters 1
2.2 MEO Observations: Moser et al. 2014, ACM 1
2.2.1 Correlation with Meteor Activity 2
2.2.2 Impact Event Parameters 2
2.2.3 Luminous Efficiency 2

3 Lunar Regolith Properties **2**

4 Spheral Benchmark of 17 March 2013 Event **2**
4.1 Getting Started and Running on Computer Clusters 2
4.1.1 Installing on MEO Cluster 2
4.1.2 Running on MEO Cluster 3
4.1.3 Running on LLNL Cluster 3
4.2 Porosity ϕ_0 Study 5
4.3 Max Strength Y_m Study 5

5 Spheral Based Lunar Ejecta Modeling **5**

6 MEM3 Based Lunar Ejecta Modeling **5**
6.1 Algorithm 5
6.2 Regolith Size Distribution 6
6.3 Ejected Mass from an Impactor 8
6.4 Meteoroid Projectile Mass Distribution 9

6.5 Meteoroid Projectile Density Distribution 10
6.6 Meteoroid Projectile Speed and Angle Distribution 12
6.7 Secondary Ejecta Distance, Speed, & Angle 13
6.7.1 Coriolis Force 15

7 NASA SP-8013 Meteoroid Environment Model - 1969 **15**

References **18**

List of Figures

1 Example of a simple excavation crater, http://keith.aa.washington.edu/craterdata/scaling/index.htm. 1
2 Geotechnical particle size distribution: midlle curve showing the average distribution; left-hand and right-hand curves showing ± 1 standard deviation [*Carrier III*, 2003]. 6
3 Non-linear fit of Figure 2 (the average distribution) with Eq. 1 in SciDAVis, giving the constants for a, b, c, and d. 7
4 Linear fit to the integrand $x^3 P_{moon}(x)$. 8
5 The Grün interplanetary meteoroid flux as a function of limiting particle mass [*Moorhead et al.*, 2019, Figure 1]. 9
6 Non-linear fit of Figure 5 with Eq. 11 in SciDAVis, giving the constants for a, b, c, and d. 10
7 Meteoroid density distribution according to the MEM3 User Guide. The apex and toroidal meteoroid sources constitute the low-density population, while the helion/antihelion source constitutes the high-density population. Each set of densities follows a log-normal distribution [c.f. Figure 11, *Moorhead et al.*, 2019]. 11
8 Non-linear fit of the low density profile in Figure 7 with Eq. 14 in SciDAVis, giving the constants for $a \rightarrow A$, $s \rightarrow \sigma$, and $m \rightarrow \mu_\delta$. 12
9 Non-linear fit of the high density profile in Figure 7 with Eq. 14 in SciDAVis, giving the constants for $a \rightarrow A$, $s \rightarrow \sigma$, and $m \rightarrow \mu_\delta$. 12
10 Average cumularive lunar ejecta flux-mass distribution for each of three ejecta velocity intervals [*Cour-Palais*, 1969]. 17

List of Tables

1 Executive Summary

2 Characteristics of the 17 March 2013 Event

2.1 LRO Observations: Robinson et al. 2015

Here we summarize the findings from *Robinson et al.* [2015]. Their assessment used the impact-scaling model of *Holsapple* [1993] to constrain the impact event parameters, with a fixed rim-to-rim crater diameter.

2.1.1 Crater Morphology

The March 2013 crater has a rim-to-rim diameter of $D_{rim} = 18.8^{+1.1}_{-1.2}$ m with a depth of approximately 2-3 m. The transient crater diameter was estimated to be $D = 14$ m, see Figure 1 for an illustration.

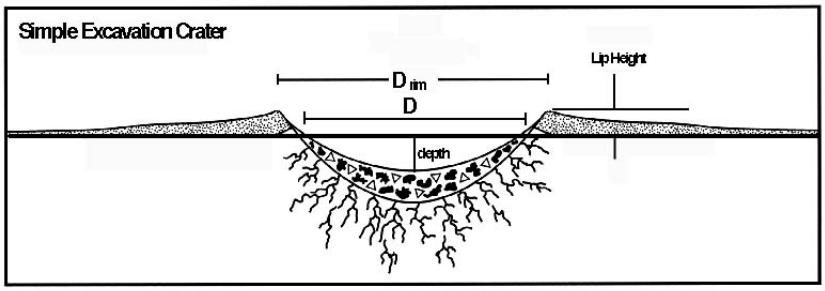

Figure 1: Example of a simple excavation crater, http://keith.aa.washington.edu/craterdata/scaling/index.htm.

2.1.2 Impact Event Parameters

Impactor densities were chosen to be either cometary 1 g/cm^3, chondritic 3.4 g/cm^3, or iron-nickle 6 g/cm^3 with plausible impact velocities of 5-60 km/s. The diameter of the impactor was between 0.28 and 1.10 m with a mass between 33 and 702 kg. For this given range of impact velocities and densities, the kinetic energy of the impactor was between 6.4×10^9 J and 6.0×10^{10} J.

2.2 MEO Observations: Moser et al. 2014, ACM

Here we summarize the findings from *Moser et al.* [2014]. They used both Gault's crater scaling law [*Gault*, 1974] and Holsapple's online calculator [*Holsapple*, 1993] in their analysis.

2.2.1 Correlation with Meteor Activity

Moser et al. [2014] found correlation with the Virginid meteor shower complex (EVI/NVI) with an observed meteor shower on 17 March 2013 and the lunar impact that was seen by NASA MSFC. According to the Meteor Data Center, the eta Virginids, EVI, have a speed of 26.6 km/s to 34.2 km/s and the Northern March Virginids, NVI, have a speed of 23.0 km/s. However, given the cluster of five fireballs that were seen on 17 March 2013, the speed was $v_g = 25.6 \pm 0.8$ km/s and matched closer to the EVI orbital elements. The Tisserand number was 3.1 ± 0.2, which is right on the line of being either cometary (< 3) or asteroidal (> 3). It was found that the lunar impact angle from the horizontal was $\theta_h = 56°$ for a Virginid meteor.

2.2.2 Impact Event Parameters

Assuming a regolith density of $\rho_t = 1500$ kg/m^3, a porosity of 40%, and cohesion strength of 0.1 Mpa, the impactor densities ranged from 1000 kg/m^3 to 3300 kg/m^3, the mass was between 11 kg and 66 kg, and the kinetic energy ranged from 3.6×10^9 J to 2.2×10^{10} J. The duration of the impact was estimated to be 1.03 s with a nominal diameter of 22 ± 3 cm, assuming $\rho_p = 3000$ kg/m^3.

2.2.3 Luminous Efficiency

From *Moser et al.* [2014], if we assume the impactor was associated with the Virginids, the luminous efficiency η_λ is in the range $7.5^{+4.5}_{-2.5} \times 10^{-4} < \eta_\lambda < 1.5^{+0.8}_{-0.5} \times 10^{-3}$, depending on the regolith density, 1500 kg/m$^3 < \rho_t < 2100$ kg/m^3, and impactor density, 1000 kg/m$^3 < \rho_t < 3300$ kg/m^3. This range of luminous efficiencies is consistent with *Bouley et al.* [2012] ($\eta_\lambda = 5 \times 10^{-4}$) and *Moser et al.* [2011] ($\eta_\lambda = 1.3 \times 10^{-3}$).

3 Lunar Regolith Properties

4 Spheral Benchmark of 17 March 2013 Event

4.1 Getting Started and Running on Computer Clusters

4.1.1 Installing on MEO Cluster

```
References:
If gcc is too old, follow this if you have CentOS:
https://ahelpme.com/linux/centos7/how-to-install-new-gcc-and-
    development-tools-under-centos-7/


To install Spheral and test installation:

cd
mkdir Spheral
```

```
mkdir github-Spheral
cd github-Spheral
git clone https://github.com/jmikeowen/spheral
cd spheral/src/
scl enable devtoolset-7 bash
./boot
mkdir BUILD
cd BUILD
../configure --prefix=/home/adestefa/Spheral --with-opt=3 --
    with-compilers=gnu --with-dbc=none
make -j 20
cd /home/adestefa/github-Spheral/spheral/tests
/home/adestefa/Spheral/bin/ats -n 20 -e /home/adestefa/Spheral
    /bin/python integration.ats



To install VisIt:

cd
mkdir download-visit
cd download-visit/
wget http://portal.nersc.gov/project/visit/releases/2.13.3/
    visit2_13_3.linux-x86_64-rhel7.tar.gz
wget http://portal.nersc.gov/project/visit/releases/2.13.3/
    visit-install2_13_3
chmod 755 visit-install2_13_3
./visit-install2_13_3 2.13.3 linux-x86_64-rhel7 /home/adestefa
    /visit-2.13.3
cd
echo "export PATH=$PATH:/home/adestefa/visit-2.13.3/bin" >> .
    bashrc
```

4.1.2 Running on MEO Cluster

4.1.3 Running on LLNL Cluster

The connection and login details described below is assumed to be on a Windows machine.

1. Connect to VPN using Cisco AnyConnect Secure Mobility Client
   - VPN name: vpn.llnl.gov
   - Group name: llnl.vpnc
2. Login with OUN (destefano2) and CZ PIN + token # (RSA SecurID)
3. SSH into LLNL server head node using Putty

- Host name: rzgw.llnl.gov
- Option: Connection → SSH → X11 → Enable X11 forwarding[1]
- Option: X display location → localhost:0
- Login: LC username (destefan)
- Password: RZ PIN + token # (RZ)

4. SSH into RZ specific server
   - ssh -XY destefan@rztopaz
   - Password: RZ PIN + token # (RZ)
5. Check current jobs for a user
   - squeue -u <username>
   - Add - -start to see begin ETA
6. Load Spheral module
   - ml Spheral/exp
7. Debug Spheral Python script
   - srun -n <# of CPUs, max 36 per node> -p pdebug python -i <python_script.py>
   - Add any variable definitions after the python_script.py, such as - -impactAngle=56, - -rImpactor=25.2, etc. See the halfSphere_amdvX.py file for more variable options.
8. Grab compute nodes for continuous debugging
   - mxterm <# of nodes, max 8> <# of CPUs, =36×# of nodes, max 288> <time, max 60 (minutes)> -q pdebug
   - After nodes have been grabbed, do steps 6 and 7 as before
9. Submit batch script
   - msub <script.msub>
10. Check drive space quota
    - quota -v

[1] Need to download either VcXsrv (works better), or Xming. In VcXsrv, which will be called VLaunch on the desktop, need to deselect **Native opengl** on the last tab.

4.2 Porosity ϕ_0 Study

4.3 Max Strength Y_m Study

5 Spheral Based Lunar Ejecta Modeling

6 MEM3 Based Lunar Ejecta Modeling

The Meteoroid Engineering Model (MEM) describes the sporadic meteoroid complex, or the background meteoroid environment, and does not include meteor showers. The impactor masses range from 1 μg to 10 g. Larger impactor masses must be dealt with differently [e.g., see *Neukum et al.*, 2001; *Brown et al.*, 2002], *which we omit here for now*[2]. We use output from MEM in order to estimate the number of particles per area per year greater than a certain mass (or the particle flux mass spectrum) due to secondary ejecta from meteoroid impacts on the Moon. The risk due to impacts on the Moon is driven by secondary ejecta and not the primary meteoroid flux.

We begin by first describing the algorithm at which we plan to use to compute the particle flux mass spectrum at a given point on the Moon. In essence, the algorithm is based on the reverse Monte-Carlo idea. We then go into detail about how to compute each step of the algorithm, either borrowing from the literature or making our own derivations.

6.1 Algorithm

1. For a given location on the Moon, compute the particle flux mass spectrum
2. For each source location
   - Defines the distance D from the source required to compute the ejecta velocity $v = v(D, \gamma)$.
3. For each ejecta angle γ
   - Completely defines the ejecta velocity $v = v(D, \gamma)$
4. For each meteoroid impact angle α (from MEM output)
   - At the moment, we will sum over the azimuthal angle and assume isotropic azimuthal seconday ejecta (this is not the case for impact angles less than 30° from the horizon).
5. For each meteoroid impact speed U
6. For each impactor density δ
   - We only need to compute this once for each target material, and can factor out as a constant. The density is given as an output in MEM.

[2] At some point we will need to account for impactor masses larger than 10 g in order to understand the tail of the distribution in terms of the risk analysis.

7. For each impactor mass m_p
   - We can integrate this out. At first glance, we will get a list of hypergeometric functions, but we only need to evaluate these once and factor out as a constant. The mass distribution is given in MEM Eq. (2.1).
8. For each ejecta particle size m_e
   - We can integrate the particle size distribution, but we will need to keep track of each mass size m_e.

6.2 Regolith Size Distribution

For relatively small impact sizes (craters $< 30 - 50$ m), we can generally assume the secondary ejecta follows that of the original regolith. The cumulative distribution function (CDF) of the particle sizes can be fit to many observations, as shown in Figure 2.

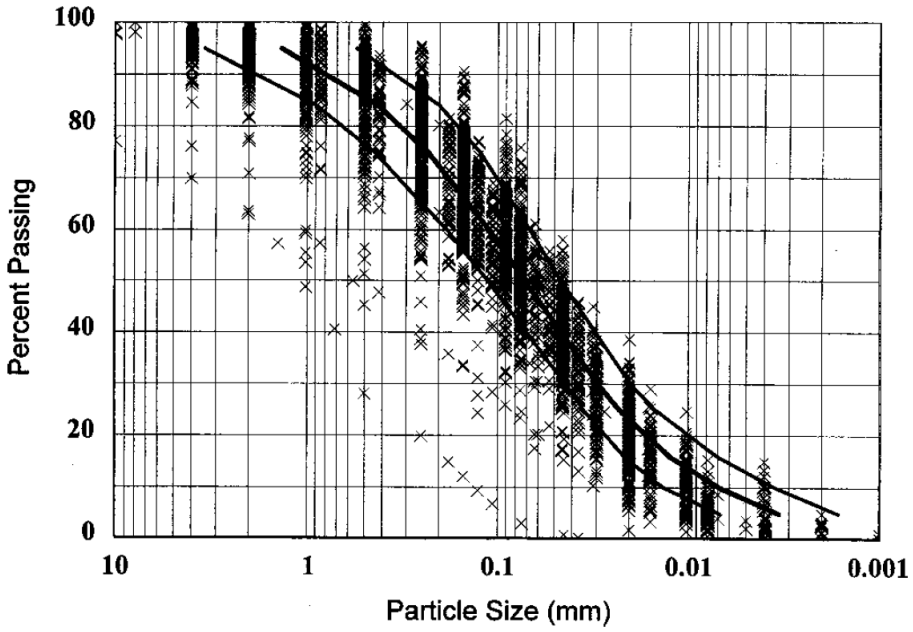

Figure 2: Geotechnical particle size distribution: midlle curve showing the average distribution; left-hand and right-hand curves showing ± 1 standard deviation [*Carrier III*, 2003].

In order to parametrize the CDF from Figure 2, we make a fit to the model equation

$$C_{moon} = 1 - \exp\left(\frac{-1}{ax^b + cx^d}\right), \tag{1}$$

which is an exponential distribution with two scales defined by a and c, with x in units of mm. In SciDAVis, we make the fit with the x-axis on a logarithmic scale to give equal weight to both small and large scaled particles. The results for the curve fit are shown in Figure 3. We found that a simple exponential distribution with a single scale was insufficient, hence the reason we opted for a two-scaled exponential distribution.

```
[12/30/2019 5:40:09 PM          Plot: "Graph2"]
Non-linear fit of dataset: Table2_2, using function: 100*(1-exp(-1/(a*(10^x)^b+c*(10^x)^d)))
Y standard errors: Unknown
Nelder-Mead Simplex algorithm with tolerance = 0.0001
From x = -2.482108151 to x = 0.134259956
a  = 0.0548044684398436 +/- 0.00569348851446585
b  = -1.01472478485333 +/- 0.0196858460040614
c  = 0.337499285612252 +/- 0.0049924392579481
d  = -0.251808155531636 +/- 0.0188844274561765
--------------------------------------------------------------------------------
Chi^2 = 8.25978651917647
R^2 = 0.999849854428033
--------------------------------------------------------------------------------
Iterations = 89
Status = success
--------------------------------------------------------------------------------
```

Figure 3: Non-linear fit of Figure 2 (the average distribution) with Eq. 1 in SciDAVis, giving the constants for a, b, c, and d.

To compute the probability distribution function (PDF), we can simply take the derivative of the CDF with respect to x, which results in the following equation:

$$P_{moon} = -A\frac{abx^{b-1} + cdx^{d-1}}{(ax^b + cx^d)^2} \exp\left(\frac{-1}{ax^b + cx^d}\right), \tag{2}$$

where A is the normalization constant. In theory, this should be equal to 1, but since we are not taking our particle size from 0 to infinity, we need to compute the value of A. If we assume the particle size can range from 0.001 mm to 10 mm, then $A = 1.02218$.

Since our goal is to compute the particle flux mass spectrum, we need to *count* the number of particles from the PDF that make up the mass of M from Eq. 6. We first need to know the total volume per complete PDF, which is given by

$$V_{P_{moon}}(x_{min}) = \frac{4}{3}\pi \int_{x_{min}}^{x_{max}} dx x^3 P_{moon}(x), \tag{3}$$

where $x_{min} = 0.001$ mm and $x_{max} = 10$ mm. An exact analytic solution of Eq. 3 is quite difficult, but we notice that the integrand $x^3 P_{moon}(x)$ very closely resembles a linear equation within the desired range, see Figure 4.

Therefore, we make the approximation

$$x^3 P_{moon}(x) \sim p_0 x + p_1, \tag{4}$$

where $p_0 = 1/11.48$ and $p_1 = 1/232.6$. The total volume of particles with mass greater

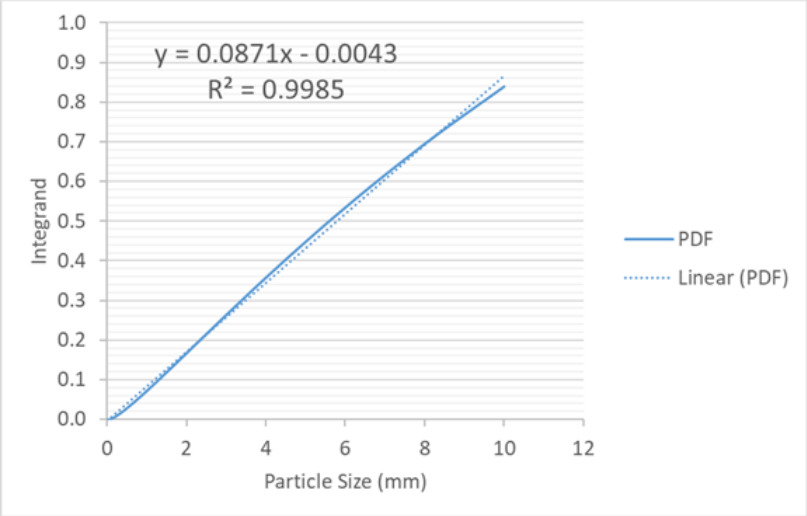

Figure 4: Linear fit to the integrand $x^3 P_{moon}(x)$.

than $m_0 = \frac{4}{3}\pi\rho x_0^3$ is given by

$$V_{P_{moon}}(x_0) = \frac{4}{3}\pi \left[\frac{1}{22.96}\left(x_{max}^2 - x_0^2\right) - \frac{1}{232.6}\left(x_{max} - x_0\right) \right], \tag{5}$$

where $V_{P_{moon}}(x_{min}) = 18.06377$ mm^3. Given the density of the regolith ρ, we can then compute the total mass of the particles from the PDF.

6.3 Ejected Mass from an Impactor

From *Housen and Holsapple* [2011], we can compute the mass ejected faster than v in terms of impactor properties, given by

$$M(v;\rho;m,\delta,U,\alpha) = C_4 m \left[\frac{v}{U\Theta(\alpha)} \left(\frac{\rho}{\delta}\right)^{\frac{3\nu-1}{3\mu}} \right]^{-3\mu}, \tag{6}$$

where

- v: secondary ejecta speed,
- ρ: target density,
- m: projectile mass,
- δ: projectile density,
- U: projectile speed,
- α: projectile impact angle (from horizon),

and

$$C_4 = \frac{3k}{4\pi} C_1^{3\mu}, \tag{7}$$

where the constants k, C_1, ν, and μ depend on the specific material properties, see Table 3 of *Housen and Holsapple* [2011]. The impact angle modification equation $\Theta(\alpha)$ can be chosen to be

$$\Theta(\alpha) = \begin{cases} 1 \\ \sin\alpha \\ \sin(\sqrt{\alpha_0^2 + \alpha^2}), \ \alpha_0 \sim 5^\circ - 15^\circ. \end{cases} \tag{8}$$

6.4 Meteoroid Projectile Mass Distribution

From the MEM3 User Guide , we get the $g(m)$ flux of meteoroids larger than a limiting mass m, originally from *Grün et al.* [1985]. The Grün interplanetary flux equation is given by

$$g(m) = (c_4 m^{\gamma_4} + c_5)^{\gamma_5} + c_6(m + c_7 m^{\gamma_6} + c_8 m^{\gamma_7})^{\gamma_8} + c_9(m + c_{10} m^{\gamma_9})^{\gamma_{10}}, \tag{9}$$

where the constants are $c_4 = 2.2 \times 10^3$, $c_5 = 15$, $c_6 = 1.3 \times 10^{-9}$, $c_7 = 10^{11}$, $c_8 = 10^{27}$, $c_9 = 1.3 \times 10^{-16}$, $c_{10} = 10^6$; and the exponents are $\gamma_4 = 0.306$, $\gamma_5 = -4.38$, $\gamma_6 = 2$, $\gamma_7 = 4$, $\gamma_8 = -0.36$, and $\gamma_{10} = -0.85$. Eq. 9 is applied to MEM's mass range and is shown in Figure 5.

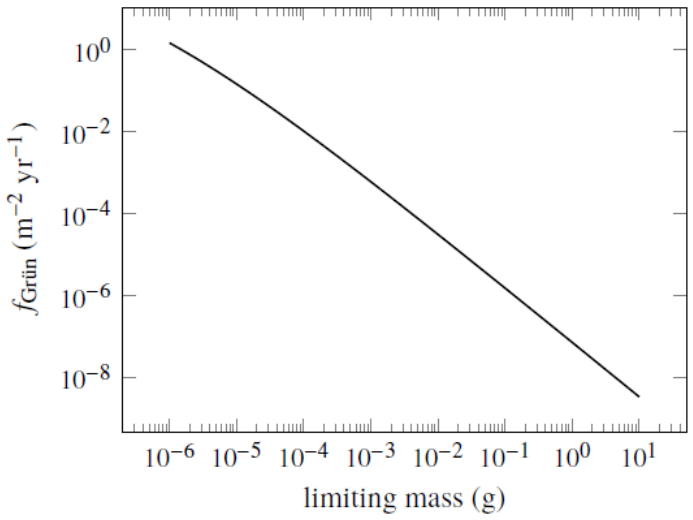

Figure 5: The Grün interplanetary meteoroid flux as a function of limiting particle mass [*Moorhead et al.*, 2019, Figure 1].

The mass flux $dg(m)/dm$ and Eq. 6 should be integrated over the mass range $m_{min} = 10^{-6}$ g to $m_{max} = 10^{1}$ g in order to account for all impactor mass sizes, which we call G_m given as

$$G_m = \int_{m_{min}}^{m_{max}} dm \frac{dg(m)}{dm} m. \tag{10}$$

The mass flux $dg(m)/dm$ can be fit to a double power law

$$\frac{dg(x)}{dx} = \frac{1}{ax^b + cx^d}, \tag{11}$$

where the fit parameters are shown in Figure 6, using a log-log scale to capture the small and large masses correctly.

```
---------------------------------------------------------------------------
[1/2/2020 4:13:33 PM          Plot: "Graph4"]
Non-linear fit of dataset: Table2_2, using function: log10(1/(a*(10^x)^b+c*(10^x)^d))
Y standard errors: Unknown
Nelder-Mead Simplex algorithm with tolerance = 0.0001
From x = -5.924382925 to x = 0.935617075
a  = 321,865,117,982,837 +/- 0
b  = 2.32111297269978 +/- 0.0005958076665748
c  = 1,406,901,447,961.14 +/- 0
d  = 1.81651108891357 +/- 0.00063978048941211
---------------------------------------------------------------------------
Chi^2 = 0.00183119809759917
R^2 = 0.999998212686885
---------------------------------------------------------------------------
Iterations = 95
Status = success
---------------------------------------------------------------------------
```

Figure 6: Non-linear fit of Figure 5 with Eq. 11 in SciDAVis, giving the constants for a, b, c, and d.

To integrate Eq. (10), we use the following solutions

$$\int dx \frac{x}{ax^b + cx^d} = -\frac{1}{a(b-2)x^{b-2}} {}_2F_1 \left[1, \frac{b-2}{b-d}; \frac{b-2}{b-d} + 1; -\frac{c}{a}x^{d-b}\right], \tag{12}$$

$$= -\frac{1}{c(d-2)x^{d-2}} {}_2F_1 \left[1, \frac{d-2}{d-b}; \frac{d-2}{d-b} + 1; -\frac{a}{c}x^{b-d}\right], \tag{13}$$

where Eq. 12 is more appropriate for small x if $d-b > 0$ and Eq. 13 is more appropriate for large x if $d - b > 0$. If the sign of $d - b$ is flipped, then the small and large scale equations are swapped.

6.5 Meteoroid Projectile Density Distribution

The meteoroid density has two components, a low and a high density contribution, as shown in Figure 7. To take into account this particular distribution in computing the

particle flux mass spectrum, we should integrate Figure 7 against Eq. 6. Since the meteoroid density components can be written in terms of log-normal distributions

$$F_\delta(x) = \frac{A}{\sigma\sqrt{2\pi}x} \exp\left[-\frac{(\ln x - \mu_\delta)^2}{2\sigma^2}\right], \tag{14}$$

the integration entails computing the moments of a log-normal distribution. The α-moment is given by

$$F_\delta^\alpha(A, \mu_\delta, \sigma) = A \exp\left(\alpha\mu_\delta + \frac{1}{2}\alpha^2\sigma^2\right). \tag{15}$$

Inserting these results into Eq. 6, the functional form of the projectile density contribution can be written as

$$F_\delta = F_\delta^{3\nu-1}(A_{low}, \mu_{low}, \sigma_{low}) + F_\delta^{3\nu-1}(A_{high}, \mu_{high}, \sigma_{high}), \tag{16}$$

where the fit parameters for the low and high density components are shown in Figures 8 and 9. Since the meteoroid density is given in units of *fraction per 50 kg m*$^{-3}$, we need to divide the A constants by 50 in order to give correct units.

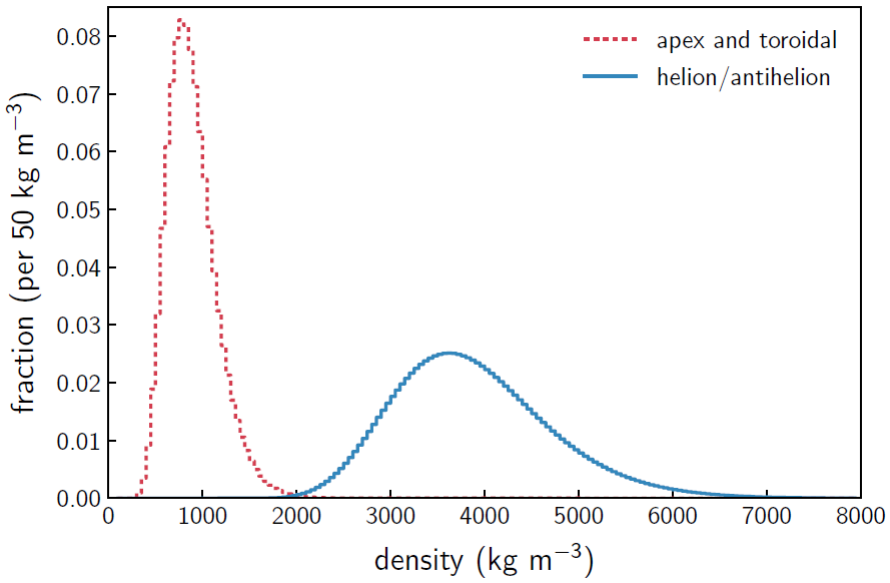

Figure 7: Meteoroid density distribution according to the MEM3 User Guide. The apex and toroidal meteoroid sources constitute the low-density population, while the helion/antihelion source constitutes the high-density population. Each set of densities follows a log-normal distribution [c.f. Figure 11, *Moorhead et al.*, 2019].

```
[1/2/2020 5:16:00 PM          Plot: "Graph5"]
Non-linear fit of dataset: Table3_2, using function: log10(a/((10^x)*s*2.506628275)*exp(-(x*ln(10)-m)^2/(2*s^2)))
Y standard errors: Unknown
Scaled Levenberg-Marquardt algorithm with tolerance = 0.0001
From x = 2.097 to x = 3.902
a  = 53.839135327051 +/- 0.82189223780795
s  = 0.294917539134767 +/- 0.000210957288819632
m  = 6.7346464600191 +/- 0.00131007263737737
Chi^2 = 0.305039664208057
R^2 = 0.999894109124399
Iterations = 0
Status = success
```

Figure 8: Non-linear fit of the low density profile in Figure 7 with Eq. 14 in SciDAVis, giving the constants for $a \to A$, $s \to \sigma$, and $m \to \mu_\delta$.

```
[1/2/2020 5:19:18 PM          Plot: "Graph6"]
Non-linear fit of dataset: Table4_2, using function: log10(a/((10^x)*s*2.506628275)*exp(-(x*ln(10)-m)^2/(2*s^2)))
Y standard errors: Unknown
Scaled Levenberg-Marquardt algorithm with tolerance = 0.0001
From x = 2.096910013 to x = 3.901730692
a  = 39.742506482046 +/- 1.58430260083343
s  = 0.221066131940955 +/- 0.00039359322394943
m  = 8.26026111215463 +/- 0.00352064330966803
Chi^2 = 5.98458401110512
R^2 = 0.999293469696896
Iterations = 0
Status = iteration is not making progress towards solution
```

Figure 9: Non-linear fit of the high density profile in Figure 7 with Eq. 14 in SciDAVis, giving the constants for $a \to A$, $s \to \sigma$, and $m \to \mu_\delta$.

6.6 Meteoroid Projectile Speed and Angle Distribution

MEM3 gives the incoming meteoroid flux (in units of # per km^2 per year) in terms of the speed U and both azimuth θ and altitude ϕ angles for a location on the Moon. At the moment, since we are assuming azimuthally symmetric ejecta, we will sum over all θ azimuthal angles to simplify our calculation. In the future, we plan to incorporate azimuthal dependence for oblique impacts by including the azimuthal dependence of the ejecta blanket. The ϕ angle in MEM3 corresponds to our α angle, which is the impact angle with respect to the horizon. There are 36 ϕ bins[3] and 40 speed bins, after integrating over the 72 θ bins for each ϕ bin.

[3]Half of the ϕ bins will always be zero, since they are below the horizon, so they can be ignored.

6.7 Secondary Ejecta Distance, Speed, & Angle

We would like to relate the distance from the meteorite impact to the secondary ejecta impact site by the secondary ejecta speed v and angle γ from zenith. If we assume the Moon is a perfect sphere with no atmosphere, we can calculate this distance by following the elliptical path the ejecta makes. The semi-major axis and eccentricity of the elliptical orbit are given by[4]

$$\frac{a}{r_m} = \frac{1}{2\left(1 - \frac{v^2}{v_{esc}^2}\right)}, \tag{17}$$

where $r_m = 1737.1$ km is the radius of the Moon and $v_{esc} = 2.38$ km/s is the Moon's escape velocity, and

$$e = \sqrt{\left(\frac{2v^2}{v_{esc}^2} - 1\right)^2 \sin^2\gamma + \cos^2\gamma}, \tag{18}$$

where we employed the fact that the gravity of the Moon is $g = GM/r_m^2$ and the escape velocity is related by $v_{esc} = \sqrt{2gr_m}$. The third equation we need gives the location in the elliptical orbit by the angle β from the perilune, the semi-major axis a, and the eccentricity e by

$$r = \frac{a(1-e^2)}{1 + e\cos\beta}. \tag{19}$$

Solving for $\cos\beta$ in Eq. 19, we have

$$\cos\beta = \frac{1}{e}\left(\frac{a(1-e^2)}{r} - 1\right). \tag{20}$$

In addition, we also need the equation for $\sin\beta$, which is given by (using a right triangle)

$$\sin\beta = \frac{1}{e}\sqrt{e^2 - \left[\frac{a(1-e^2)}{r} - 1\right]^2}, \tag{21}$$

so that $\tan\beta$ is

$$\tan\beta = \frac{\sqrt{e^2 - \left[\frac{a(1-e^2)}{r} - 1\right]^2}}{\frac{a(1-e^2)}{r} - 1}. \tag{22}$$

We found that the distance the secondary ejecta travels is given by the arc length of Moon the orbit travels greater than the radius of the Moon:

$$D = 2(\pi - \beta)r_m, \tag{23}$$

or solving for the angle β,

$$\beta = \pi - \frac{D}{2r_m}. \tag{24}$$

[4] See Eqs. 4.30 and 4.32 from http://www.braeunig.us/space/orbmech.htm.

Using Eqs. 17 and 18, we can write

$$\frac{a}{r_m}(1-e^2) = 2\frac{v^2}{v_{esc}^2}\sin^2\gamma, \tag{25}$$

so Eq. 22 becomes [c.f., Eq. (1) of *Vickery*, 1986]

$$\tan\left(\frac{D}{2r_m}\right) = \frac{2\frac{v^2}{v_{esc}^2}\sin\gamma\cos\gamma}{1-2\frac{v^2}{v_{esc}^2}\sin^2\gamma}. \tag{26}$$

For $D \ll 2r_m$, the optimum angle that gives the smallest velocity needed is $45°$. In other words, for a given velocity, the greatest distance is found by taking $\gamma = 45°$. However, if the distance D is roughly the same order as the diameter of the Moon $2r_m$, ($D > 0.01 \times 2r_m$), then the optimal angle from zenith is greater than $45°$, i.e. a shallower angle to the horizon. This is because at large velocities, the curvature of the Moon comes into play. For larger velocities, there are also angles γ that cannot reach a distance D. Allowable angles (in radians) that can travel a distance D are defined by

$$\gamma > \frac{D}{4r_m}. \tag{27}$$

In other words, the maximum distance the ejecta can reach for a given angle is

$$D = 4\gamma r_m. \tag{28}$$

For example, from this equation we can conclude that for $\gamma < 45°$, the ejecta will not reach the antipodal point.

Solving for v we have

$$\frac{v}{v_{esc}} = \frac{+1}{\sqrt{\sin(2\gamma)\left(\cot\left(\frac{D}{2r_m}\right)+\tan\gamma\right)}}. \tag{29}$$

We can also solve for the zenith angle γ, given by

$$\cot\gamma = x^2\cot\left(\frac{D}{2r_m}\right) \pm \sqrt{x^4\cot^2\left(\frac{D}{2r_m}\right)+(2x^2-1)}, \tag{30}$$

where $x = v/v_{esc}$. Solving for the discriminant, the minimum x can be for a given distance D is

$$x_{min}^2 = \tan^2\left(\frac{D}{2r_m}\right)\left[\csc\left(\frac{D}{2r_m}\right)-1\right]. \tag{31}$$

Plugging into Equation 30, the optimal angle from zenith is given by

$$\cot\gamma_{opt} = \sec\left(\frac{D}{2r_m}\right) - \tan\left(\frac{D}{2r_m}\right). \tag{32}$$

Once $D > \pi r_m$, the optimal angle is $\gamma = 90°$, i.e., parallel to the horizon. For small distances $D \ll 2r_m$, the optimal angle is $\gamma = 45°$, as mentioned above.

6.7.1 Coriolis Force

The Coriolis force on secondary ejecta may also affect the ground path. To estimate the strength of the Coriolis force, the greatest speed due to the rotation of the Moon is at the equator, given by

$$v_c = \frac{2\pi r_m}{T} = \frac{2\pi * 1737.1 \text{ km}}{27.322 \text{ days}} = 4.62 \text{ m/s}. \tag{33}$$

Therefore, we can ignore the Coriolis force if the ejecta speed v is greater than roughly $\sim 10 - 15 \times v_c$, or about 46 m/s to 70 m/s. This translates into ejecta distances less than 3 km, which at those small distances the Coriolis force should not cause an effect anyways. So in general, we conclude that we can ignore the Coriolis force all together.

To quantify this conclusion, let us compute the Rossby number

$$R_o = \frac{v}{fL}. \tag{34}$$

If we assume an ejecta angle of $45°$, then plotting D as a function of v in Eq. 26 shows that $D \to L \sim v^2$. Taking our example above for $v = 70$ m/s, $L = 3$ km, and $f = 2T$ to solve for A, we find that the Rossby number for secondary ejecta on the Moon is

$$R_o = \frac{A}{fv}, \tag{35}$$

where $A = 1.63$ m/s^2[5], $f = 5.328 \times 10^{-6}$ rad/s, and v is in units of m/s. In order to have $R_o \sim 1$ (small R_o means the Coriolis forces cannot be ignored), we would need $v > 306$ km/s, which far exceeds the escape speed. The smallest R_o can ever be is $R_o \sim 128$ when taking $v \to v_{esc}$. Therefore, we feel confident in our omission of the Coriolis force.

7 NASA SP-8013 Meteoroid Environment Model - 1969

The NASA SP-8013 Meteoroid Environment Model [*Cour-Palais*, 1969], is a document published in 1969 that describes the meteoroid and lunar ejecta environment of cometary origin with masses between 10^{-12} g and 1 g. The flux-mass models and the associated density and velocity characteristics are for engineering applications in the design of space vehicles for near-Earth orbit, cis-lunar, lunar orbit, and lunar surface missions.

Our aim is to provide an updated specification to NASA SP-8013 for the lunar impact ejecta environment. Until the update is finished, DSNE points to Figure 10 (shown here in Figure 10) of *Cour-Palais* [1969] for lunar ejecta. The results that follow from Sections 5 and 6 will be verified against NASA SP-8013. We already anticipate that our new environments will be more benign (e.g., [*Bjorkman and Christiansen*, 2019, pointing out that 50 J is the critial energy]), however to what degree from our analysis is yet to be determined. We also plan to provide output in terms of penetrating

flux as a function of critical kinetic energy, as comparison to Figure 5 of *Bjorkman and Christiansen* [2019], to aid in risk assessment of lunar impact ejecta.

Our ultimate goal in providing an updated environment definition is to have an output in the same format as MEM 3's igloo files (see Section 3.4.4 of *Moorhead et al.* [2019]). This will allow for current analysis tools already familiar with MEM 3 to ingest our new environments without modification to those tools.

[5] Curiously, this is basically the acceleration due to gravity on the Moon.

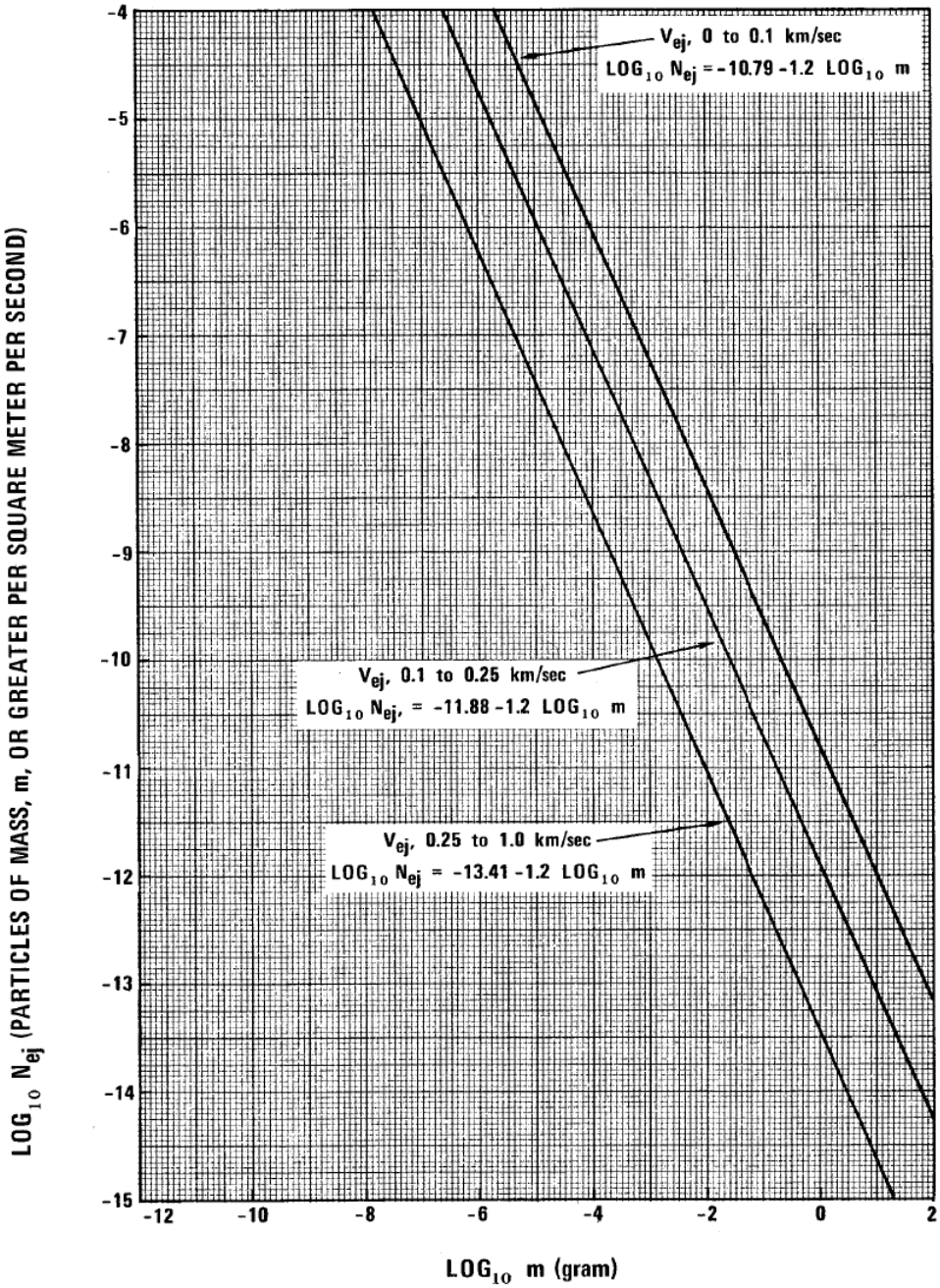

Figure 10: Average cumularive lunar ejecta flux-mass distribution for each of three ejecta velocity intervals [*Cour-Palais*, 1969].

References

Bjorkman, M. D., and E. L. Christiansen, An astronaut's risk of experiencing a critical impact from lunar ejecta during lunar eva, 2019.

Bouley, S., et al., Power and duration of impact flashes on the moon: Implication for the cause of radiation, *Icarus*, *218*(1), 115–124, 2012.

Brown, P., R. Spalding, D. O. ReVelle, E. Tagliaferri, and S. Worden, The flux of small near-earth objects colliding with the earth, *Nature*, *420*(6913), 294, 2002.

Carrier III, W. D., Particle size distribution of lunar soil, *Journal of Geotechnical and Geoenvironmental Engineering*, *129*(10), 956–959, 2003.

Cour-Palais, B. G., Meteoroid environment model 1969 (near earth to lunar surface), nasa sp-8013, *National Aeronautics and Space Administration, Washington, DC*, 1969.

Gault, D. E., Impact cratering, in *A primer in lunar geology*, 1974.

Grün, E., H. Zook, H. Fechtig, and R. Giese, Collisional balance of the meteoritic complex, *Icarus*, *62*(2), 244–272, 1985.

Holsapple, K., The scaling of impact processes in planetary sciences, *Annual review of earth and planetary sciences*, *21*(1), 333–373, 1993.

Housen, K. R., and K. A. Holsapple, Ejecta from impact craters, *Icarus*, *211*(1), 856–875, 2011.

Moorhead, A. V., A. Kingery, and S. Ehlert, Nasas meteoroid engineering model 3 and its ability to replicate spacecraft impact rates, *Journal of Spacecraft and Rockets*, pp. 1–17, 2019.

Moser, D., R. Suggs, W. Swift, R. Suggs, W. Cooke, A. Diekmann, and H. Koehler, Luminous efficiency of hypervelocity meteoroid impacts on the moon derived from the 2006 geminids, 2007 lyrids, and 2008 taurids, *Meteoroids: The Smallest Solar System Bodies*, p. 142, 2011.

Moser, D., R. Suggs, and R. Suggs, Large meteoroid impact on the moon on 17 march 2013, in *Asteroids, Comets, Meteors 2014*, 2014.

Neukum, G., B. A. Ivanov, and W. K. Hartmann, Cratering records in the inner solar system in relation to the lunar reference system, in *Chronology and evolution of Mars*, pp. 55–86, Springer, 2001.

Robinson, M. S., et al., New crater on the moon and a swarm of secondaries, *Icarus*, *252*, 229–235, 2015.

Vickery, A., Size-velocity distribution of large ejecta fragments, *Icarus*, *67*(2), 224–236, 1986.